DNA Interaction of the Tyrosine Protein Kinase Inhibitor PD153035 and Its *N*-Methyl Analogue†

Jean-François Goossens,‡ Edith Bouey-Bencteux,§ Raymond Houssin,§ Jean-Pierre Hénichart,§ Pierre Colson,|| Claude Houssier,|| William Laine,⊥ Brigitte Baldeyrou,⊥ and Christian Bailly*,⊥

Laboratoire de Chimie Analytique, Faculté des Sciences Pharmaceutiques et Biologiques, and Institut de Chimie Pharmaceutique Albert Lespagnol (EA2692), Université de Lille 2, 59006 Lille, France, Laboratoire de Chimie Macromoléculaire et Chimie Physique, Institut de Chimie, Université de Liège, Sart-Tilman (B6), 4000 Liège, Belgium, and Laboratoire de Pharmacologie Antitumorale du Centre Oscar Lambret-INSERM U-524, IRCL, Place de Verdun, 59045 Lille, France

Received December 6, 2000; Revised Manuscript Received February 6, 2001

ABSTRACT: The brominated anilinoquinazoline derivative PD153035 exhibits a very high affinity and selectivity for the epidermal growth factor receptor tyrosine kinase (EGF-R TK) and shows a remarkable cytotoxicity against several types of tumor cell lines. In contrast, its *N*-methyl derivative, designated EBE-A22, has no effect on EGF-R TK but maintains a high cytotoxic profile. The present study was performed to explore the possibility that PD153035 and its *N*-methyl analogue might interact with double-stranded DNA, which is a primary target for many conventional antitumor agents. We studied the strength and mode of binding to DNA of PD153035 and EBE-A22 by means of absorption, fluorescence, and circular and linear dichroism as well as by a relaxation assay using human DNA topoisomerases. The results of various optical and gel electrophoresis techniques converge to show that both drugs bind to DNA and behave as typical intercalating agents. In particular, EBE-A22 unwinds supercoiled plasmid, stabilizes duplex DNA against heat denaturation, and produces negative CD and ELD signals, as expected for an intercalating agent. Extensive DNase I footprinting experiments performed with a large range of DNA substrates show that EBE-A22, but not PD153035, interacts preferentially with GC-rich sequences and discriminates against homooligomeric runs of A and T which are often cut more readily by the enzyme in the presence of the drug compared to the control. Altogether, the results provide the first experimental evidence that DNA is a target of anilinoquinazoline derivatives and suggest that this *N*-methylated ring system is a valid candidate for the development of DNA-targeted cytotoxic compounds. The possible relevance of selective DNA binding to activity is considered. The unexpected GC-selective binding properties of EBE-A22 entreat further exploration into the use of *N*-methylanilinoquinazoline derivatives as tools for designing sequence-specific DNA binding ligands.

The epidermal growth factor (EGF) receptor tyrosine kinase (hereafter designed EGF-R TK)[1] represents an attractive target for the development of new series of antitumor agents. A small number of drugs designed to target the EGF-R TK have recently entered clinical testing as antitumor drugs, and the results reported so far are encouraging. The observation that the EGF-R is overexpressed in several tumor types has raised hope that small molecules directed against this receptor might act as cancer-specific bullets and therefore might reduce or eliminate the unwanted cytotoxic effects associated with conventional cancer chemotherapy (*1*).

The EGF-R TK inhibitors tested clinically as antitumor agents include the quinazoline derivatives ZD1839 (AstraZeneca) and CP358774 (Pfizer) and the pyrrolopyrimidine derivative CGP59326 (Novartis). All major pharmaceutical companies are currently developing tyrosine-specific protein kinase inhibitors (*2, 3*). In the EGF-R TK series, one of the most potent compounds is the brominated quinazoline PD153035 (Figure 1, Parke-Davis), which exhibits a sharp selectivity and a tremendously high affinity for the EGF receptor ($K_i = 5$ pM) coupled with a remarkable cytotoxicity against several types of tumors in vitro such as the A431 epidermoid carcinoma cell line ($IC_{50} = 29$ pM) (*4*). Despite its poor efficacy in vivo and the fact that it is insoluble in water, the discovery of this compound greatly stimulated the search for other EGF-R TK inhibitors and as such contributed significantly to a better understanding of the EGF-mediated signal transduction pathways.

† This work was supported by research grants (to C.H. and P.C.) from Actions de Recherches Concertées Grant 95/00-93, and (to J.-P.H. and C.B.) from the Ligue Nationale Française Contre le Cancer (Comité du Nord). Support by the "convention INSERM-CFB" is acknowledged.

* Address correspondence to this author. Tel: (+33) 320 16 92 18; Fax: (+33) 320 16 92 29; E-mail: bailly@lille.inserm.fr.

‡ Laboratoire de Chimie Analytique, Université de Lille 2.

§ EA2692, Université de Lille 2.

|| Laboratoire de Chimie Macromoléculaire et Chimie Physique, Université de Liège.

⊥ Laboratoire de Pharmacologie Antitumorale du Centre Oscar Lambret-INSERM U-524.

[1] Abbreviations: CD, circular dichroism; EGF-R TK, epidermal growth factor receptor tyrosine kinase; ELD, electric linear dichroism; TBE, Tris−borate−EDTA.

10.1021/bi002777a CCC: $20.00
Published on Web 03/17/2001

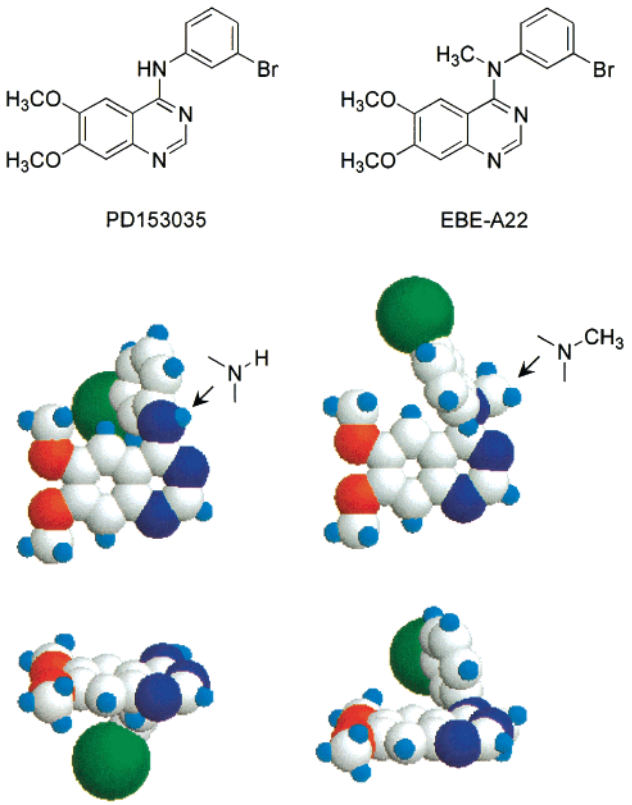

FIGURE 1: Structures of PD153035 and its *N*-methyl analogue EBE-A22. Energy-minimized structures of the drugs are shown. The softwares HyperChem 5.01 and Alchemy 2000 were used to construct the structures.

The design and synthesis of hundreds of analogues of PD153035 have helped elucidate the structure−activity relationships in the anilinoquinazoline series of EGF-R TK inhibitors. Second-generation inhibitors equipped with solubilizing groups have been successfully developed and are currently being subjected to preclinical testing (*5*). However, the newly designed "soluble-153035" analogues do not exhibit the exceptional potency of the parent compound.

PD153035 and its tumor-active analogue CP358774 both contain an anilinoquinazoline core which is essential to EGF-R TK activity (*6*,*7*). Methylation of the amino group separating the two heterocycles leads to compounds totally inactive in both the EGF-R kinase assay and the cellular EGF-R autophosphorylation assay (*8*, *9*). Nevertheless, *N*-methylanilinoquinazoline derivatives can maintain a significant cytotoxicity (*9*,*10*). In particular, it was observed that the *N*-methyl analogue of PD153035, named EBE-A22 in Figure 1, retained good anti-proliferative activity despite its total absence of EGF-R TK inhibitory effect (*11*). These considerations prompted us to search for an alternative molecular target. In particular, we explored the possibility that DNA might represent a target for the *N*-methyl analogue of PD153035, as is the case for many conventional antitumor agents.

MATERIALS AND METHODS

Chemicals and Biochemicals. The synthesis of PD153035 and EBE-A22 has been reported (*11*). In both cases, a 5 mM stock solution was prepared in DMSO, and subsequent dilutions were made in aqueous buffer. Calf thymus DNA and the double-stranded polymers poly(dA-dT)$_2$ and poly(dG-dC)$_2$ were from Pharmacia (Uppsala, Sweden). Their concentrations were determined by applying molar extinction coefficients of 6600, 6600, and 8400 M^{-1} cm^{-1}, respectively (*12*). Calf thymus DNA was deproteinized with sodium dodecyl sulfate (protein content <0.2%), and all nucleic acids were dialyzed against 1 mM sodium cacodylate buffered solution, pH 7.0. The nucleoside triphosphate labeled with ^{32}P (α-dATP) was obtained from Amersham (Buckinghamshire, England) (3000 Ci/mmol). Restriction endonucleases and AMV reverse transcriptase were purchased from Boehringer (Mannheim, Germany) and used according to the supplier's recommended protocol in the activity buffer provided. All other chemicals were analytical grade reagents.

Absorption Spectroscopy and Melting Temperature Studies. Absorption spectra and melting curves were measured using an Uvikon 943 spectrophotometer coupled to a Neslab RTE111 cryostat. Titrations of the drug with DNA, covering a large range of DNA-phosphate/drug ratios (P/D), were performed by adding aliquots of a concentrated DNA solution to a drug solution at constant ligand concentration (20 μM). For each series of T_m measurements, 12 samples were placed in a thermostatically controlled cell holder, and the quartz cuvettes (10 mm path length) were heated by circulating water. The measurements were performed in BPE buffer, pH 7.1 (6 mM Na_2HPO_4, 2 mM NaH_2PO_4, 1 mM EDTA). The temperature inside the cuvette was measured with a platinum probe; it was increased over the range 20−100 °C with a heating rate of 1 °C/min. The "melting" temperature, T_m, was taken as the midpoint of the hyperchromic transition.

Fluorescence Titration Experiments. Fluorescence titration data were recorded at room temperature using a SPEX fluorometer Fluorolog. Excitation was at 360 nm, and fluorescence emission was monitored over the range 380−520 nm. Samples used for titration experiments were prepared separately at a constant drug concentration of 5 μM, and DNA concentrations ranging from 0.1 μM to 1 mM bp. Fluorescence titration data were fitted directly to get binding constants using a fitting function incorporated into Prism 3.0.

Circular Dichroism. CD spectra were recorded on a Jobin-Yvon CD 6 dichrograph interfaced to a microcomputer. Solutions of drugs, nucleic acids, and their complexes (3 mL in 1 mM sodium cacodylate buffer, pH 7.0) were scanned in 2 cm quartz cuvettes. Measurements were made by progressive dilution of drug−DNA complex at a high P/D (phosphate/drug) ratio with a pure ligand solution to yield the desired drug/DNA ratio. Four scans were accumulated and automatically averaged.

Electric Linear Dichroism. ELD measurements were performed with a computerized optical measurement system using the procedures previously outlined (*13*). All experiments were conducted with a 10 mm path length Kerr cell having 1.5 mm electrode separation. The samples were oriented under an electric field strength varying from 1 to 14 kV/cm. The drug under test was present at 10 μM concentration together with the DNA at 200 μM concentration unless otherwise stated. This electrooptical method has proved most useful to determine the orientation of the drugs bound to DNA. It has the additional advantage that it senses only the orientation of the polymer-bound ligand: free ligand is isotropic and does not contribute to the signal (*14*).

DNA Relaxation Experiments. Supercoiled pKMp27 DNA (0.5 μg) was incubated with 4 units of human topoisomerase

I or II (TopoGen Inc.) at 37 °C for 1 h in relaxation buffer (50 mM Tris, pH 7.8, 50 mM KCl, 10 mM $MgCl_2$, 1 mM dithiothreitol, 1 mM EDTA) in the presence of varying concentrations of the drug under study. Reactions were terminated by adding SDS to 0.25% and proteinase K to 250 μg/mL. DNA samples were then added to the electrophoresis dye mixture (3 μL) and electrophoresed in a 1% agarose gel at room temperature for 2 h at 120 V. Gels were stained with ethidium bromide (1 μg/mL), washed, and photographed under UV light. Similar experiments were performed using ethidium-containing agarose gels.

DNA Purification and Radiolabeling. Plasmids pBS (Stratagene), pTayB (kindly provided by Dr. N. E. Møllegaard, The Panum Institute, Copenhagen, Denmark), and pLAZ3 (*15*) were isolated from *E. coli* by a standard sodium dodecyl sulfate−sodium hydroxide lysis procedure and purified by banding in CsCl−ethidium bromide gradients. Ethidium was removed by several 2-propanol extractions followed by exhaustive dialysis against Tris−EDTA buffered solution. The purified plasmid was then precipitated and resuspended in the appropriate buffered medium prior to digestion by the restriction enzymes. The two pBS DNA fragments were prepared by 3′-^{32}P-end-labeling of the *Eco*RI−*Pvu*II double digest of the plasmid using [α-^{32}P]-dATP and AMV reverse transcriptase. Similarly, the 156-mer and 178-mer fragments were prepared by 3′-end-labeling of the *Eco*RI−*Hin*dIII and *Eco*RI−*Pvu*II digests, respectively, of plasmid pLAZ3. The 131-mer was obtained from plasmid pTayB after digestion with *Eco*RI and *Hin*dIII. In each case, the labeled digestion products were separated on a 6% polyacrylamide gel under nondenaturing conditions in TBE buffer (89 mM Tris−borate, pH 8.3, 1 mM EDTA). After autoradiography, the requisite band of DNA was excised, crushed, and soaked in elution buffer (500 mM ammonium acetate, 10 mM magnesium acetate) overnight at 37 °C. This suspension was filtered through a Millipore 0.22 μm filter, and the DNA was precipitated with ethanol. Following washing with 70% ethanol and vacuum-drying of the precipitate, the labeled DNA was resuspended in 10 mM Tris adjusted to pH 7.0 containing 10 mM NaCl.

DNase I Footprinting. Experiments were performed essentially as previously described (*16*). Briefly, reactions were conducted in a total volume of 10 μL. Samples (3 μL) of the labeled DNA fragments were incubated with 5 μL of the buffered solution containing the ligand at appropriate concentration. After 30 min incubation at 37 °C to ensure equilibration of the binding reaction, the digestion was initiated by the addition of 2 μL of a DNase I solution whose concentration was adjusted to yield a final enzyme concentration of about 0.01 unit/mL in the reaction mixture. After 3 min, the reaction was stopped by freeze-drying. Samples were lyophilized and resuspended in 5 μL of an 80% formamide solution containing tracking dyes. The DNA samples were then heated at 90 °C for 4 min and chilled in ice for 4 min prior to electrophoresis.

Electrophoresis and Quantitation by Storage Phosphor Imaging. DNA cleavage products were resolved by polyacrylamide gel electrophoresis under denaturating conditions (0.3 mm thick, 8% acrylamide containing 8 M urea). After electrophoresis (about 2.5 h at 60 W, 1600 V in Tris−borate−EDTA buffered solution, BRL sequencer model S2), gels were soaked in 10% acetic acid for 10 min, transferred to Whatman 3MM paper, and dried under vacuum at 80 °C. A Molecular Dynamics 425E PhosphorImager was used to collect data from the storage screens exposed to dried gels overnight at room temperature. Baseline-corrected scans were analyzed by integrating all the densities between two selected boundaries using ImageQuant version 3.3 software. Each resolved band was assigned to a particular bond within the DNA fragments by comparison of its position relative to sequencing standards generated by treatment of the DNA with dimethyl sulfate followed by piperidine-induced cleavage at the modified guanine bases in DNA (G-track).

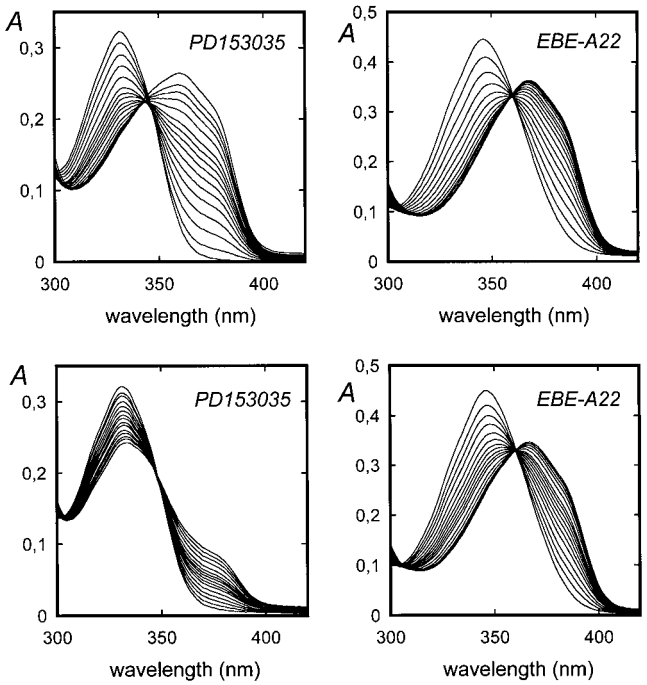

FIGURE 2: DNA titrations of PD153035 and EBE-A22 in (top) the low-salt (1 mM sodium cacodylate buffer) and (bottom) medium-salt (BPE: 6 mM Na_2HPO_4, 2 mM NaH_2PO_4, 1 mM Na_2EDTA) buffers at pH 7.0. To 3 mL of drug solution at 20 μM were added aliquots of a concentrated calf thymus DNA solution. The phosphate-DNA/drug ratio increased as follows (top to bottom curves, at 367 nm): 0, 0.2, 0.4, 0.6, 0.8, 1, 1.25, 1.5, 1.75, 2, 3, 4, 6, 8, 10, 12, 14, 16, 20.

RESULTS

The binding of PD153035 and its *N*-methyl analogue to DNA was studied by different methods to evaluate the spectroscopic changes of the anilinoquinazoline chromophore and the structural changes of the double helix. Figure 2 displays the titration of calf thymus DNA into a buffered aqueous solution of the drugs. Absorption measurements were performed in a classical phosphate buffer (BPE buffer, 16 mM Na^+) and in a low ionic strength buffer (1 mM cacodylate) required for lineEBE-A22ar dichroism measurements. In both cases, addition of DNA induces marked changes of the absorption spectra of PD153035 and EBE-A22. In the low-salt buffer, strong bathochromic and hypochromic shifts were observed with both drugs. The absorption maximum of PD153035 is shifted from 332 to 362 nm, and the red-shift amounts to 22 nm with EBE-A22 (from 346 to 368 nm). Moreover, during the titration with DNA, isosbestic points at 345 and 361 nm were detected with PD153035 and EBE-A22, respectively, pointing to the existence of a single binding mode.

Table 1: Variation in Melting Temperature (T_m, in °C)[a]

		PD153035		EBE-A22	
drug/DNA ratio	DNA alone	0.5	1	0.5	1
cacodylate buffer	45.9	49.6	50.9	71.4	74.8
BPE buffer	62.9	63	63.5	68.8	72

[a] T_m measurements were performed in BPE buffer (6 mM Na_2HPO_4, 2 mM NaH_2PO_4, 1 mM EDTA) or cacodylate buffer (1 mM sodium cacodylate) using 20 μM calf thymus DNA in 3 mL quartz cuvettes at 260 nm with a heating rate of 1 °C/min. Each drug concentration was tested in duplicate.

At a higher ionic strength (BPE buffer, 16 mM Na^+), the binding of PD153035 to DNA is reduced whereas that of EBE-A22 remains more or less unchanged. With EBE-A22, the titration shows a 20 nm bathochromic shift and a marked decrease in extinction coefficient. Under the same conditions, the spectral changes are considerably reduced with PD153035. The increase of the absorption at 370 nm is very weak compared to the changes observed during the same titration in the low-salt cacodylate buffer. However, with both drugs the interaction with DNA remains homogeneous, as judged from the presence of isosbestic points.

For EBE-A22, but not for PD153035, we were able to evaluate accurately the strength of the interaction with calf thymus DNA by fluorescence measurements. The fluorescence emission at 436 nm is weak when the drug is free in solution, but it is significantly enhanced when the drug is bound to DNA (excitation wavelength: 360 nm). This property is useful for the determination of the DNA binding affinities. Nonlinear least-squares analysis of the fluorescence titration curves (not shown) yielded binding constants of 2.14×10^4 and 1.86×10^4 $(M\ bp)^{-1}$ for EBE-A22 in BPE buffer and cacodylate buffer, respectively. In the case of PD153035, the changes of fluorescence emission at 420 nm were very weak. Under such conditions, attempts to estimate the binding constant are generally doomed to failure.

The interaction of the drugs with calf thymus DNA was also investigated by thermal denaturation analysis. Plots of absorbance at 260 nm versus temperature showed that EBE-A22 stabilizes the double helix structure of DNA whereas under the same conditions (BPE buffer) PD153035 showed no effect on the thermal stability of DNA. ΔT_m ($T_m^{\text{drug-DNA complex}} - T_m^{\text{DNA alone}}$) values of 6 and 9 °C were measured with EBE-A22 for drug/DNA-phosphate ratios of 0.5 and 1, respectively. In the BPE buffer, the T_m value of calf thymus DNA (63 °C) remained unchanged in the presence of PD153035, even at a high drug/DNA ratio. In the low ionic strength cacodylate buffer, both drugs increase the T_m of DNA, but the stabilization effect was considerably higher with EBE-A22 compared to PD153035 (Table 1). The addition of the *N*-methyl substituent on the aminoquinazoline group increases significantly the affinity of the ligand for DNA.

We investigated the effect of the drugs on the relaxation of plasmid DNA by topoisomerases. Supercoiled DNA was treated with either topoisomerase I or topoisomerase II in the presence of increasing concentrations of the test drugs. The DNA relaxation products were then resolved by agarose gel electrophoresis. Typical gels are presented in Figure 3. PD153035 has practically no effect on the unwinding of DNA mediated by human topoisomerases. In contrast, EBE-A22 induces a shift of the topoisomer distribution, indicating that this compound affects the superhelical density of the plasmid. This topoisomerization assay thus reveals that EBE-A22, but not PD153035, unwinds closed circular duplex DNA. This effect is typical of an intercalating agent and has been previously observed with conventional intercalators such as ethidium bromide and ellipticines (*17*). It should be noted also that neither PD153035 nor its *N*-methyl analogue acts as a poison for human topoisomerases; cleavage experiments indicated they do not stabilize the covalent complexes between DNA and topoisomerase I or II (data not shown).

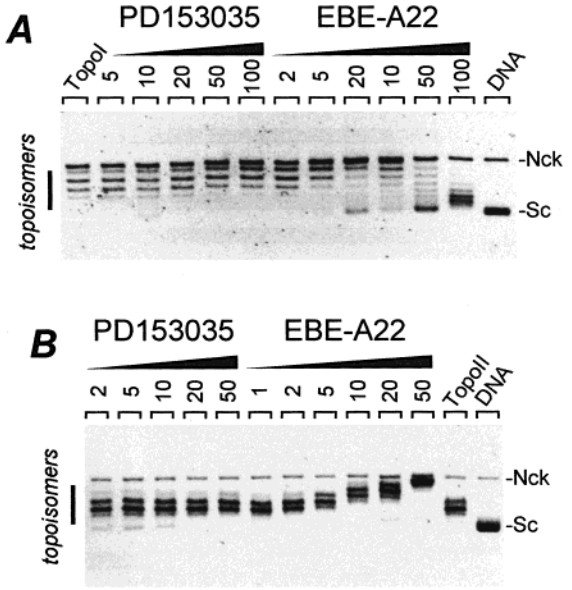

FIGURE 3: Effect of the drugs on DNA supercoiling mediated by (A) topoisomerase I and (B) topoisomerase II. Native supercoiled pAT DNA (0.5 μg) (lane DNA) was incubated for 30 min at 37 °C with 6 units of topoisomerase in the absence (lane Topo) or in the presence of drug at the indicated concentration (μM). Reaction was stopped with sodium dodecyl sulfate and treatment with proteinase K. The DNA was analyzed by native agarose gel electrophoresis. The gels were stained with ethidium bromide and photographed under UV light.

Two spectroscopic methods utilizing polarized light were applied to define more precisely the binding process for EBE-A22. Circular dichroism (CD) measurements showed that a negative band centered at 360−365 nm appeared upon addition of calf thymus DNA (Figure 4). Under identical conditions (1 mM sodium cacodylate buffer), the reduced dichroism was about 3 times more negative with EBE-A22 compared to PD153035 when the ligand is fully bound to ADN (for DNA-phosphate/drug ratio ≥ 20, data not shown). Such a weak negative induced CD is perfectly consistent with an intercalative mode of binding to DNA. Electric linear dichroism (ELD) experiments confirmed this hypothesis. Due to the high electric field applied to the DNA samples (up to 14 kV/cm), only the low ionic strength cacodylate buffer could be used for these experiments. The ELD spectra of PD153035 and EBE-A22 bound to calf thymus DNA showed a negative reduced dichroism, $\Delta A/A$, in the drug absorption band (Figure 5A). In both cases, the 300−400 nm negative band reflects the orientation of the anilinoquinazoline chromophore along the electric field. The fact that $\Delta A/A$ depends almost similarly upon the field strength for the drug−DNA complexes at 360 nm and the DNA bases at 260 nm in the absence of ligand (Figure 5B) indicates that the drug

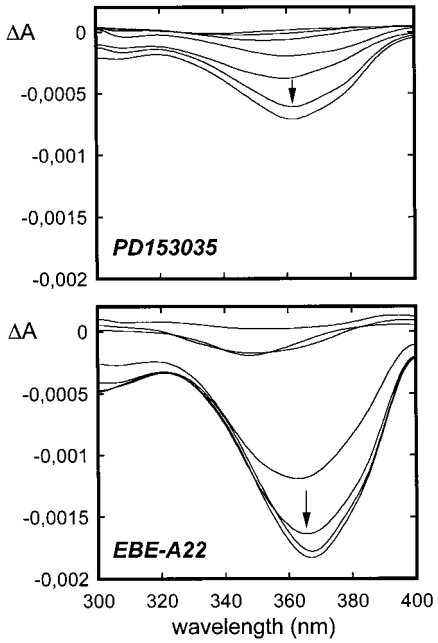

FIGURE 4: Circular dichroism titrations of PD153035 and EBE-A22 with calf thymus DNA. The DNA-phosphate/drug ratio (P/D) increased as follows (top to bottom curves at 318 nm): 1, 2.5, 5, 10, 20, 40, 50. A 3 mL solution of the drug−DNA complex at a P/D ratio of 50 was successively diluted with increasing volumes of a DNA-free solution of the test drug at a fixed concentration of 20 μM in 1 mM sodium cacodylate buffer, pH 7.0. Spectra were recorded in a 2 cm quartz cuvette.

chromophore is oriented parallel to the DNA base pairs, as expected for intercalative binding. The binding of the drugs to DNA likely induces a stiffening effect explaining the higher reduced dichroism value measured in the absorption band of the drugs than in the DNA absorption band. The two sets of spectroscopic measurements, CD and ELD, are mutually consistent and corroborate the hypothesis drawn from the unwinding data that EBE-A22 intercalates into DNA.

Additional ELD measurements were performed with the synthetic polynucleotides poly(dA-dT)$_2$ and poly(dG-dC)$_2$. Here again, the reduced dichroism measured in the drug absorption band was negative, but, interestingly, very distinct ELD spectra were recorded. The $\Delta A/A$ values were much more negative with poly(dG-dC)$_2$ than with poly(dA-dT)$_2$ (Figure 6A). With the GC polynucleotides, the field strength dependence of the reduced dichroism was absolutely identical for the polynucleotide alone and for the drug−poly(dG-dC)$_2$ complex, indicating that the drug chromophore and the base pairs are coplanar. In sharp contrast, the reduced dichroism measured with the drug−poly(dA-dT)$_2$ complex was considerably lower than that measured with poly(dA-dT)$_2$ alone. These ELD measurements suggested that the *N*-methylated anilinoquinazoline derivative exhibits a preference for GC sequences over AT ones. They also prompted us to investigate in more detail the sequence selectivity using the well-established DNase I footprinting technique.

Footprinting studies were performed using the endonuclease DNase I, which is a sensitive enzyme for mapping DNA binding sites of small molecules (*16*). Five different DNA restriction fragments of 117, 131, 156, 178, and 265 base pairs, all 3′-end-labeled, were used as substrates. A complete set of typical autoradiographs of the sequencing

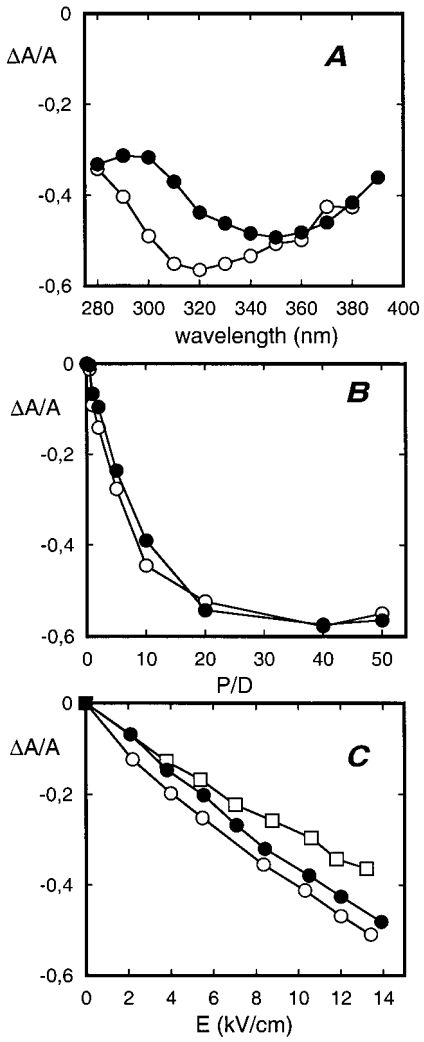

FIGURE 5: Dependence of the reduced dichroism $\Delta A/A$ on (A) the wavelength, (B) the DNA-phosphate/drug ratio (P/D), and (C) the electric field strength. (●) PD153035, (○) EBE-A22, (□) DNA alone. Conditions: (A) 13.6 kV/cm, P/D = 20 (200 μM DNA, 10 μM drug); (B) 360 nm, 13.6 kV/cm; (C) 360 nm, P/D = 20 for the DNA−drug complexes and 260 nm for the DNA alone, in 1 mM sodium cacodylate buffer, pH 7.0.

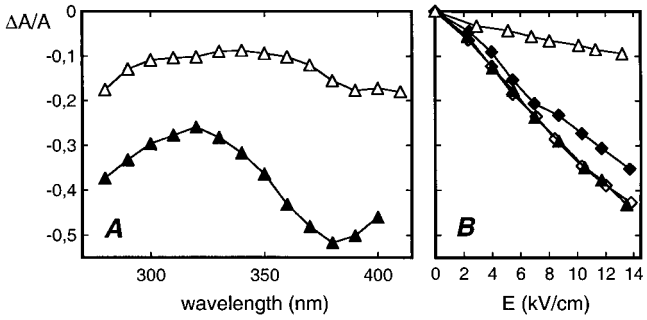

FIGURE 6: (A) ELD spectra of EBE-A22 bound to (△) poly(dA-dT)$_2$ and (▲) poly(dG-dC)$_2$. (B) Variation of the reduced dichroism $\Delta A/A$ with the electric field strength for (◆) poly(dA-dT)$_2$, (◇) poly(dG-dC)$_2$, (△) EBE-A22−poly(dA-dT)$_2$ complex, and (▲) EBE-A22−poly(dG-dC)$_2$ complex. ELD data were recorded in the presence of 200 μM polynucleotide and 20 μM drug, in 1 mM sodium cacodylate buffer, pH 7.0, under a field strength of 13.6 kV/cm.

gels used to fractionate the products of partial digestion of each DNA fragment complexed with the two test compounds is presented in Figure 7. With PD153035, there was very

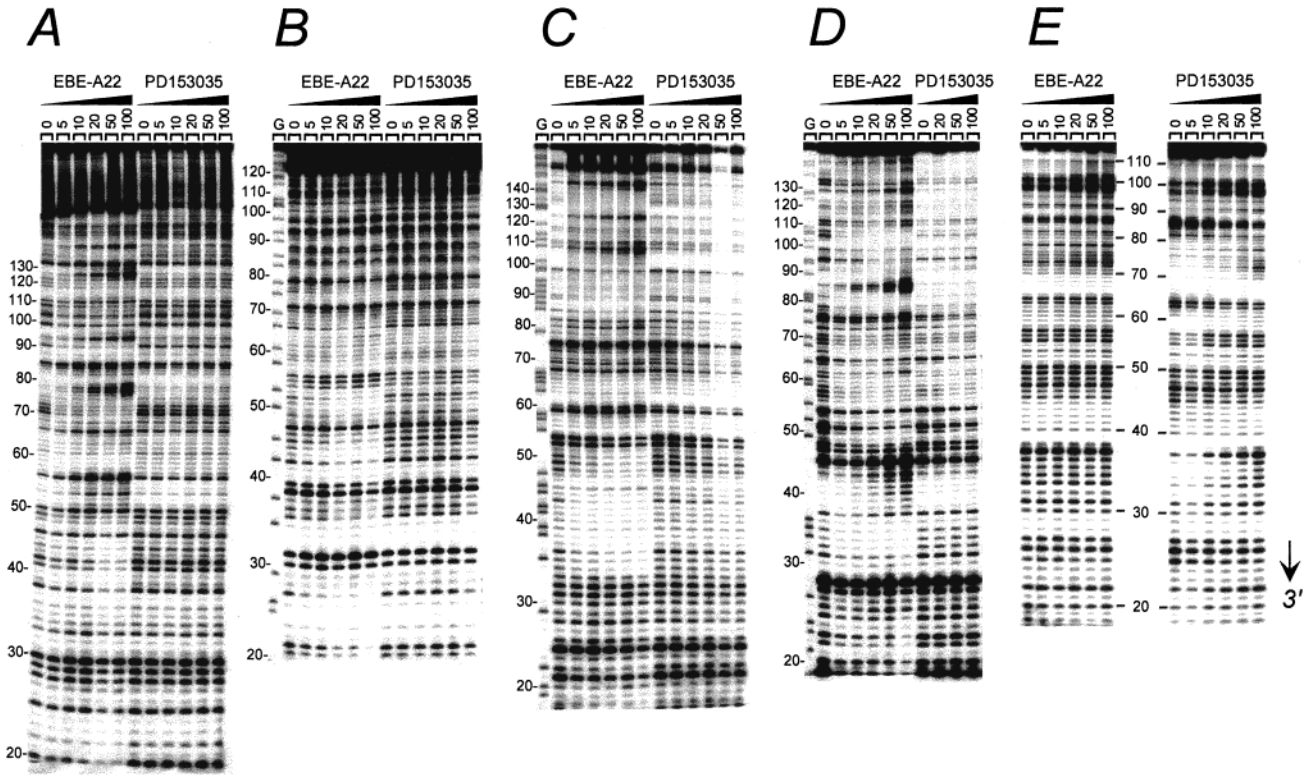

FIGURE 7: Sequence-selective binding of EBE-A22. The gels show DNase I footprinting with a series of DNA restriction fragments of (A) 265, (B) 131, (C) 178, (D) 156, and (E) 117 base pairs. The 117-mer and 265-mer *Pvu*II−*Eco*RI fragments were cut from the plasmid pBS. The 156-mer *Eco*RI−*Hin*dIII and 178-mer *Eco*RI−*Pvu*II fragments were obtained from plasmid pLAZ3. The 131-mer fragment comes from plasmid pTayB. In each case, the DNA was 3′-end-labeled at the *Eco*RI site with [α-^{32}P]dATP in the presence of AMV reverse transcriptase. The products of nuclease digestion were resolved on an 8% polyacrylamide gel containing 7 M urea. Control tracks (marked 0) contained no drug. Guanine-specific sequence markers obtained by treatment of the DNA with dimethyl sulfate followed by piperidine were run in the lanes marked G. Numbers on the side of the gels refer to the standard numbering scheme for the nucleotide sequence of the DNA fragment.

little or no inhibition of DNase I cutting whereas EBE-A22 strongly affected the cleavage of the DNA substrates by the nuclease. Visual inspection of the gels suffices to establish that the *N*-methyl compound is a sequence-selective binder. Numerous bands in the drug-containing lanes were weaker than the same bands in the drug-free lane, corresponding to attenuated cleavage, while others display relative enhancement of cutting.

A densitometric analysis of the autoradiographs obtained with the 117 and 265 bp fragments from plasmid pBS is presented in Figure 8. In the presence of EBE-A22, several regions of attenuated DNA cleavage can be discerned around positions 35, 57, and 72 (117-mer) and 43, 61, 71, and 89 (265-mer). The footprints all coincide with the position of nucleotide sequences with a high GC content, such as 5′-CGCC, 5′-CGGCCAG, and 5′-CATGCCTGC for example. PD153035 showed no such protection of GC-rich sequences, even when using a very high drug concentration (100 μM). With the *N*-methyl analogue, the footprints can be detected at 5 μM and became stronger as the drug concentration was raised to 100 μM. It should also be noted that upon binding of EBE-A22, numerous regions are rendered more susceptible to attack by DNase I than in the control. These regions of drug-induced enhanced cleavage all correspond to AT-rich sequences. For example, DNase I cutting at sequences 5′-AAAA and 5′-AAATTAA around positions 55 and 76 on the 265-mer is markedly increased in the presence of EBE-A22 (Figure 8). The cleavage enhancement at AT sites is attributable to intercalation-induced perturbations of the double-helical structure of DNA.

Similar data were obtained with the three other restriction fragments. The differential cleavage plots shown in Figure 9 confirm that EBE-A22 interacts preferentially with GC-rich sequences. All footprints (black bars in Figure 9, presumptive drug binding sites) correspond to sequences essentially composed of two or more consecutive G·C base pairs. For example, the long GC-rich sequence in the 178-mer, 5′-CTCCACCGCGGTGGCGGCCGCT, was significantly protected from DNase I cleavage in the presence of the *N*-methylated drug whereas under the same conditions PD153035 showed no effect on DNase I cleavage. As with the pBS fragments, in many cases regions corresponding to runs of A and/or T, which are generally poorly cut in the absence of drug, became much more susceptible to the cleavage in the presence of EBE-A22. Like most intercalating drugs, EBE-A22 strongly discriminates between runs of adenines or thymines. Therefore, we concluded unambiguously that the binding of the *N*-methylanilinoquinazoline derivative to GC sequences was much favored over binding to AT or mixed sequences.

DISCUSSION

This study identifies DNA as a potential target for the tyrosine protein kinase inhibitor PD153035 and its *N*-methyl analogue. We showed that these two compounds intercalate into double-stranded DNA, as is the case with a substantial

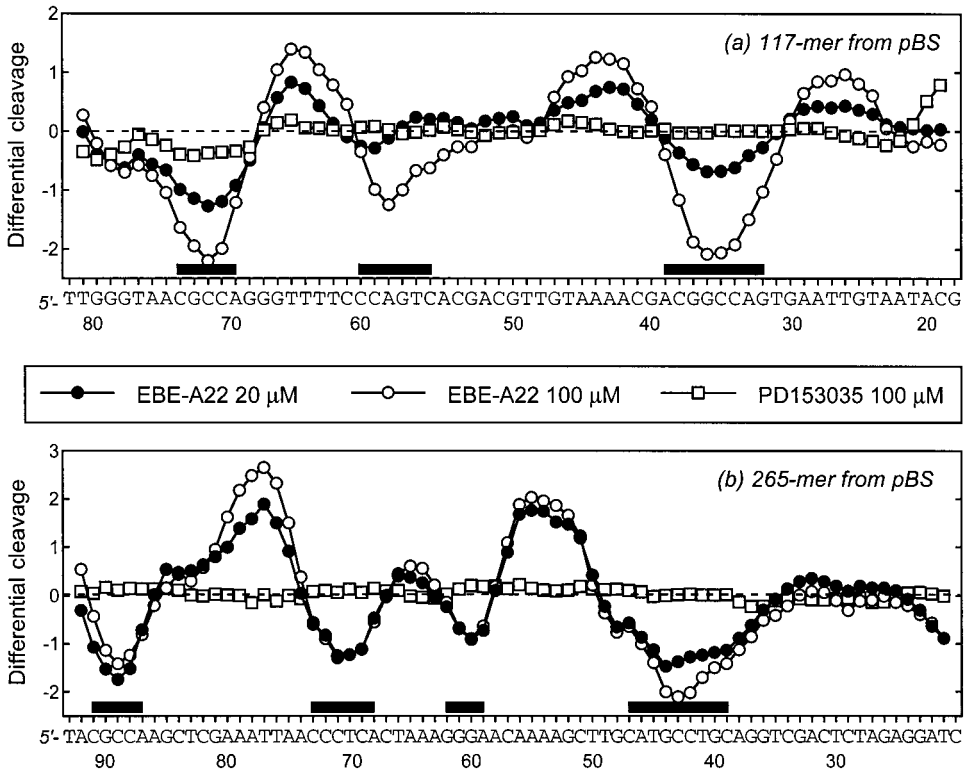

FIGURE 8: Differential cleavage plots comparing the susceptibility of the 117-mer and 265-mer DNA fragments to DNase I cutting in the presence of 20 μM and/or 100 μM PD153035 and EBE-A22. Negative values correspond to a ligand-protected site, and positive values represent enhanced cleavage. Vertical scales are in units of $\ln(f_a) - \ln(f_c)$, where f_a is the fractional cleavage at any bond in the presence of the drug and f_c is the fractional cleavage of the same bond in the control, given closely similar extents of overall digestion. Each line drawn represents a three-bond running average of individual data points, calculated by averaging the value of $\ln(f_a) - \ln(f_c)$ at any bond with those of its two nearest neighbors. Only the region of the restriction fragments analyzed by densitometry is shown. Black boxes indicate the positions of inhibition of DNase I cutting in the presence of EBE-A22.

proportion of the clinically useful anticancer drugs. The affinity of the *N*-methylated anilinoquinazoline derivative EBE-A22 for DNA is relatively weak (at least 1 order of magnitude lower) compared to that of classical intercalators such as ethidium bromide or daunomycin but comparable to that of other uncharged intercalating agents such as rebeccamycin-type indolocarbazoles for example (*18, 19*). It was known that methylation of the anilino nitrogen of PD153035 destroys affinity for EGF-R TK (*5*), but it was totally unexpected that this somewhat subtle change could facilitate the interaction of the drug with DNA and confer sequence selectivity.

The absorption, CD, and ELD spectroscopic data all indicate that PD153035 can interact with DNA, at least in a low-salt buffer. At a higher ionic strength, the binding is significantly reduced, but, nevertheless, the interaction can still be detected. The T_m measurements indicate that methylation of the anilino nitrogen reinforces significantly the interaction with DNA and interestingly confers a marked preference for GC-rich sequences. The footprinting data in Figures 7−9 provide the first experimental evidence that an *N*-methylanilinoquinazoline compound is capable of recognizing specific DNA sequences. The progressive change in the footprinting pattern seen with EBE-A22 over a large range of drug concentrations (from 5 to 100 μM) argues in favor of the involvement of sequence-specific binding to different sites which are occupied according to their relative affinities rather than drug-induced changes in DNA conformation. We find that EBE-A22 strongly discriminates against AT-rich sequences and manifests a general preference for GC-rich sites in DNA. This behavior is immediately reminiscent of the preference of typical intercalators which are often GC selective (*20*). These include actinomycin (*21*), certain ellipticines (*22*), and indoloquinoline alkaloids (*23*). But the footprints obtained with EBE-A22 are much more pronounced that those observed previously with these drugs. The protection pattern found for EBE-A22 also differs from that produced by the intercalating agents daunomycin (*24*) and ethidium (*25*), both of which exhibit a more or less pronounced GC selectivity. Among all the drugs that have been footprinted with DNase I (*26*), we found that the observed specificity of EBE-A22 most closely resembles the pattern reported for acridine-4-carboxamide derivatives, which are well-characterized intercalators (*27, 28*). For example, the amsacrine-4-carboxamide SN16713 produces a pattern of protection most similar to that observed with EBE-A22 (*29, 30*). Interestingly, SN16713 and EBE-A22 both contain an anilino ring which is at considerable angles to the planar ring system, acridine or quinazoline (*31*). This significant structural similarity is consistent with the similar DNA binding results obtained with these two compounds.

The reason EBE-A22, but not PD153035, exhibits a sharp GC preference remains unclear at present although it is obvious that the *N*-methyl group is absolutely essential to the GC-selectivity. It is likely that this substituent reduces the conformational flexibility of the molecule and thus helps to maintain the anilinoquinazoline chromophore in a specific conformation favorable for intercalation into DNA and G·C base pair recognition. According to our preliminary modeling

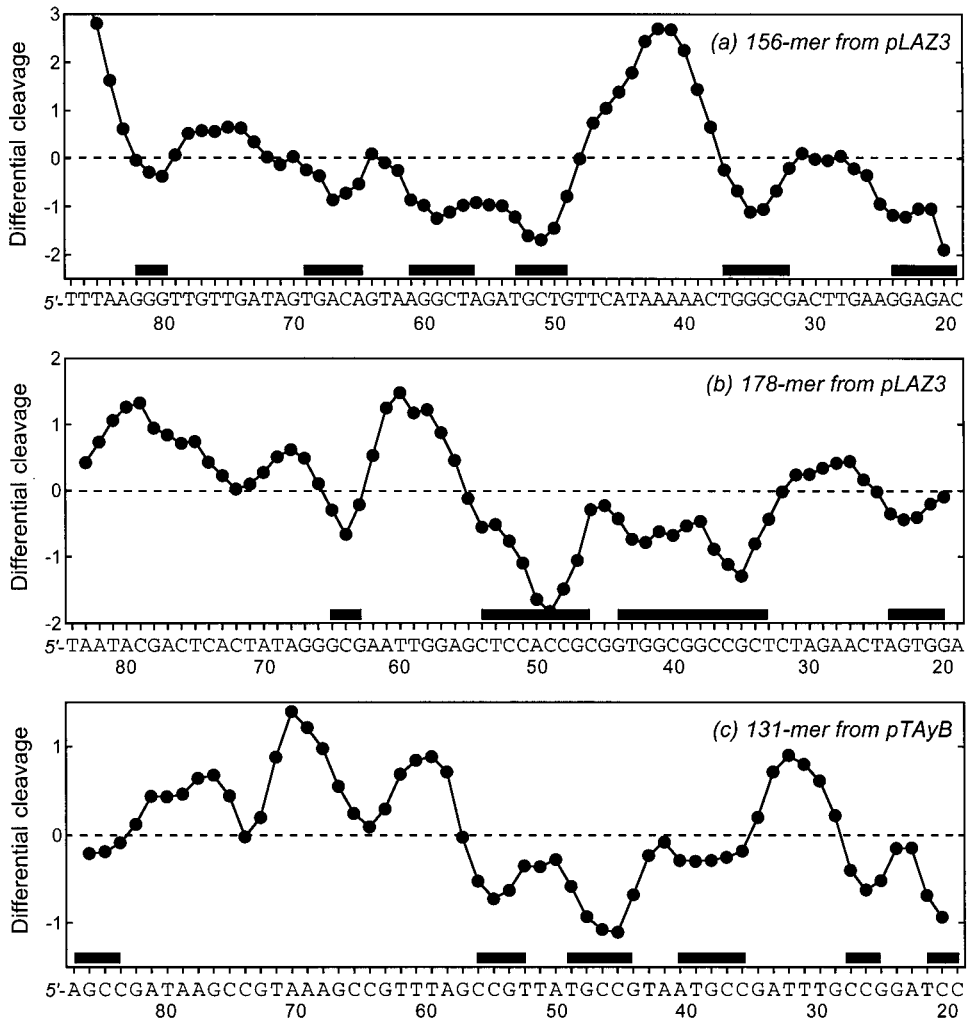

FIGURE 9: Differential cleavage plots comparing the susceptibility of the 156-, 178-, and 131-mer DNA fragments to DNase I cutting in the presence of 50 μM EBE-A22. Other details as for Figure 8.

analysis, the presence of the *N*-methyl group favors an L-shape conformation where the anilino group is almost perpendicular to the plane of the quinazoline ring (Figure 1). In contrast, the conformation of PD153035 would be more extended. These two most stable conformations are totally consistent with those deduced from NMR measurements with the related NH and N-Me anilinoquinazoline derivatives RPR-108518A and RPR-108514A, inhibitors of different tyrosine kinases (*9*). The X-ray structure of another closely related anilinoquinazoline derivative (for which the Br atom of PD153035 has been replaced with an OH group) revealed that in the CDK2 complex, the phenyl ring was approximately coplanar with the quinazoline ring system (*32*). We postulate that the intercalation of the quinazoline ring of EBE-A22 between two consecutive base pairs places the appended 4-bromoanilino moiety in one of the helical grooves, most likely the minor groove. It is known that DNase I enters the DNA double helix via the minor groove. In binding to DNA, the enzyme engages in contacts with two phosphates on either side of the cleaved bond and two phosphates on the other strand across the minor groove, opposite the phosphates contacted on the 5′ side of the cleaved bond (*33*−*35*). For this reason, we strongly believe that the intense footprints produced by EBE-A22 reflect direct competition with the binding and cutting of the enzyme in the minor groove.

Whether or not the GC preference of EBE-A22 has any bearing on its cytotoxic action remains to be determined, but, given the lack of effect of this compound of the EGF-R TK, it is plausible that its cytotoxic potential arises, at least in part, from its capacity to interact with DNA. The DNA binding affinity is relatively modest, but it is not necessary for DNA-interactive drugs to bind with high affinity to exert a biological effect because of the enormous effective concentration of their receptor inside cells (*36*, *37*). EBE-A22 could interfere with diverse DNA-interacting proteins such as polymerases or transcription factors. Neither PD153035 nor EBE-A22 stabilizes DNA−topoisomerase covalent complexes, but they may affect other enzymes. For example, EBE-A22 may inhibit DNA helicases, as is the case for many GC-specific intercalators (*38*).

PD153035 is not the only kinase inhibitor shown to bind to DNA. Recently, Bible and co-workers reported that flavopiridol, a highly potent cyclin-dependent kinase inhibitor, binds to duplex DNA. NMR and modeling studies suggested that this flavone derivative intercalates into DNA but with no apparent sequence preference (*39*). Flavopiridol and EBE-A22 appear to bind to DNA similarly and with roughly equal binding affinities, but only the *N*-methylanilinoquinazoline derivative presents a high selectivity for GC-rich sequences.

Although PD153035 is essentially a tyrosine kinase inhibitor (it has picomolar inhibitory effects on EGF-R kinase), it is, however, possible that its DNA binding capacity also plays a role in its biological activity. The DNA interaction discovered here may contribute to the therapeutic effect or to the unwanted cytotoxic activity. For this reason, it would be important to investigate the interaction with nucleic acids of related quinazoline-based signal transduction inhibitors targeting EGF-R, in particular ZD1839, PD0169414, and CP358774 which are currently undergoing early clinical development (*40*, *41*). In addition, it may turn valuable to design DNA-targeted *N*-methylanilinoquinazolines endowed with a pronounced selectivity for GC-rich sequences. Such compounds may reveal unexpected cytotoxic potentials. The *N*-methylanilinoquinazoline unit represents a useful chemotype for the preparation of DNA-targeted anticancer agents.

REFERENCES

1. Buolamwini, J. K. (1999) *Curr. Opin. Chem. Biol. 3*, 500−509.
2. Lawrence, D. S., and Niu, J. (1998) *Pharmacol. Ther. 77*, 81−114.
3. Toledo, L. M., Lydon, N. B., and Elbaum, D. (1999) *Curr. Med. Chem. 6*, 775−805.
4. Fry, D. W., Kraker, A. J., McMichael, A., Ambroso, L. A., Nelson, J. M., Leopold, W. R., Connors, R. W., and Bridges, A. J. (1994) *Science 265*, 1093−1095.
5. Bridges, A. J. (1999) *Curr. Med. Chem. 6*, 825−843.
6. Bridges, A. J., Cody, D. R., Zhou, H., McMichael, A., and Fry, D. W. (1995) *Bioorg. Med. Chem. 3*, 1651−1656.
7. Bridges, A. J., Zhou, H., Cody, D. R., Rewcastle, G. W., McMichael, A., Showalter, H. D. H., Fry, D. W., Kraker, A. J., and Denny, W. A. (1996) *J. Med. Chem. 39*, 267−276.
8. Rewcastle, G. W., Denny, W. A., Bridges, A. J., Zhou, H., Cody, D. R., McMichael, A., and Fry, D. W. (1995) *J. Med. Chem. 38*, 3482−3487.
9. Myers, M. R., Setzer, N. N., Spada, A. P., Persons, P. E., Ly, C. Q., Maguire, M. P., Zulli, A. L., Cheney, D. L., Zilberstein, A., Johnson, S. E., Franks, C. F., and Mitchell, K. J. (1997) *Bioorg. Med. Chem. Lett. 7*, 421−424.
10. Wakeling, A. E., Baker, A. J., Davies, D. H., Brown, D. S., Green, L. R., Cartlidge, S. A., and Woodburn, J. R. (1996) *Breast Cancer Res. Treat. 38*, 67−74.
11. Bouey-Bencteux, E., Loison, C., Pommery, N., Houssin, R., and Hénichart, J. P. (1998) *Anti-Cancer Drug Des. 13*, 893−922.
12. Wells, R. D., Larson, J. E., Grant, R. C., Shortle, B. E., and Cantor, C. R. (1970) *J. Mol. Biol. 54*, 465−497.
13. Houssier, C. (1981) in *Molecular Electrooptics* (Krause, S., Ed.) pp 363−398, Plenum Publishing Corp., New York.
14. Colson, P., Bailly, C., and Houssier, C. (1996) *Biophys. Chem. 58*, 125−140.
15. Kerckaert, J. P., Deweindt, C., Tilly, H., Quief, S., Lecocq, G., and Bastard, C. (1993) *Nat. Genet. 5*, 66−70.
16. Bailly, C., and Waring, M. J. (1995) *J. Biomol. Struct. Dyn. 12*, 869−898
17. Bailly, C., OhUigin, C., Houssin, R., Colson, P., Houssier, C., Rivalle, C., Bisagni, E., Hénichart, J. P., and Waring, M. J. (1992) *Mol. Pharmacol. 41*, 845−855.
18. Bailly, C., Qu, X., Anizon, F., Prudhomme, M., Riou, J. F., and Chaires, J. B. (1999) *Mol. Pharmacol. 55*, 377−385.
19. Bailly, C., Qu, X., Chaires, J. B., Colson, P., Houssier, C., Ohkubo, M., Nishimura, S., and Yoshinari, T. (1999) *J. Med. Chem. 42*, 2927−2935.
20. Müller, W., and Crothers, D. M. (1975) *Eur. J. Biochem. 54*, 267−277.
21. Fox, K. R., and Waring, M. J. (1984) *Nucleic Acids Res. 12*, 9271−9285.
22. Bailly, C., OhUigin, C., Rivalle, C., Bisagni, E., Hénichart, J. P., and Waring, M. J. (1990) *Nucleic Acids Res. 18*, 6283−6291.
23. Bonjean, K., De Pauw-Gillet, M.-C., Defresne, M.-P., Colson, P., Houssier, C., Dassonneville, L., Bailly, C., Greimers, R., Wright, C., Quetin-Leclercq, J., Tits, M., and Angenot, L. (1998) *Biochemistry 37*, 5136−5146.
24. Chaires, J. B., Fox, K. R., Herrera, J. E., Britt, M., and Waring, M. J. (1987) *Biochemistry 26*, 8227−8236.
25. Fox, K. R., and Waring, M. J. (1987) *Nucleic Acids Res. 15*, 491−507.
26. Waring, M. J., and Bailly, C. (1994) *J. Mol. Recognit. 7*, 109−122.
27. Adams, A., Guss, J. M., Collyer, C. A., Denny, W. A., and Wakelin, L. P. G. (1999) *Biochemistry 38*, 9221−9233.
28. Adams, A., Guss, J. M., Collyer, C. A., Denny, W. A., Prakash, A. S., and Wakelin, L. P. G. (2000) *Mol. Pharmacol. 58*, 649−658.
29. Bailly, C., Denny, W. A., Mellor, L., Wakelin, L. P. G., and Waring, M. J. (1992) *Biochemistry 31*, 3514−3524.
30. Bailly, C., Denny, W. A., and Waring, M. J. (1996) *Anti-Cancer Drug Des. 11*, 611−624.
31. Buckleton, J. S., and Waters, T. N. (1984) *Acta Crystallogr. C40*, 1587−1593.
32. Shewchuk, L., Hassell, A., Wisely, B., Rocque, W., Holmes, W., Veal, J., and Kuyper, L. F. (2000) *J. Med. Chem. 43*, 133−138.
33. Suck, D., and Oefner, C. (1986) *Nature 321*, 620−625.
34. Suck, D., Lahm, A., and Oefner, C. (1988) *Nature 332*, 465−468.
35. Weston, S. A., Lahm, A., and Suck, D. (1992) *J. Mol. Biol. 226*, 1237−1256.
36. Neidle, S., and Waring, M. J. (1983) *Molecular Aspects of Anticancer Drug−DNA Interactions*, Vol. 1 and 2, Macmillan, London.
37. Waring, M. J., and Ponder, B. A. J. (1992) *The Search for New Anticancer Drugs*, Kluwer Academic Publishers, Dordrecht.
38. Bachur, N. R., Johnson, R., Yu, F., Hickey, R., Applegren, N., and Malkas, L. (1993) *Mol. Pharmacol. 44*, 1064−1069.
39. Bible, K. C., Bible, R. H., Jr., Kottke, T. J., Svingen, P. A., Xu, K., Pang, Y.-P., Hajdu, E., and Kaufmann, S. H. (2000) *Cancer Res. 60*, 2419−2428.
40. Seymour, L. (1999) *Cancer Treat. Rev. 25*, 301−312.
41. Vincent, P. W., Bridges, A. J., Dykes, D. J., Fry, D. W., Leopold, W. R., Patmore, S. J., Roberts, B. J., Rose, S., Sherwood, V., Zhou, H., and Elliott, W. L. (2000) *Cancer Chemother. Pharmacol. 45*, 231−238.

BI002777A